

# Multimodal Generalized Zero Shot Learning For Gleason Grading Using Self-Supervised Learning

Dwarikanath Mahapatra

Inception Institute of Artificial Intelligence, UAE  
dwarikanath.mahapatra@inceptioniai.org

**Abstract.** Gleason grading from histopathology images is essential for accurate prostate cancer (PCa) diagnosis. Since such images are obtained after invasive tissue resection quick diagnosis is challenging under the existing paradigm. We propose a method to predict Gleason grades from magnetic resonance (MR) images which are non-interventional and easily acquired. We solve the problem in a generalized zero-shot learning (GZSL) setting since we may not access training images of every disease grade. Synthetic MRI feature vectors of unseen grades (classes) are generated by exploiting Gleason grades' ordered nature through a conditional variational autoencoder (CVAE) incorporating self-supervised learning. Corresponding histopathology features are generated using cycle GANs, and combined with MR features to predict Gleason grades of test images. Experimental results show our method outperforms competing feature generating approaches for GZSL, and comes close to performance of fully supervised methods.

**Keywords:** GZSL · CVAE · Gleason grading · Histopathology · MRI.

## 1 Introduction

Early and accurate diagnosis of prostate cancer (PCa) is an important clinical problem. High resolution histopathology images provide the gold standard but involve invasive tissue resection. Non-invasive techniques like magnetic resonance imaging (MRI) are useful for early abnormality detection [9, 12, 19, 28, 37, 40, 94, 133, 135, 158] and easier to acquire, but their low resolution and noise makes it difficult to detect subtle differences between benign conditions and cancer. A combination of MRI and histopathology features can potentially leverage their respective advantages for improved accuracy in early PCa detection. Accessing annotated multimodal data of same patient from same examination instance is a challenge. Hence a machine learning model to generate one domain's features from the other is beneficial to combine them for PCa detection. Current supervised learning [6, 7, 39, 54, 55, 58, 68, 79, 81, 97, 131, 165], and multiple instance learning [15, 44, 49–51, 53, 82, 98, 101, 109, 121, 123, 125, 134] approaches for Gleason grading use all class labels in training. Accessing labeled samples of all Gleason grades is challenging, and we also encounter known and unknown cases at test

time, making the problem one of generalized zero-shot learning (GZSL). We propose to predict Gleason grades for PCa by generating histopathology features from MRI features and combining them for GZSL based disease classification.

GZSL classifies natural images from seen and unseen classes [10, 13, 16, 29, 34, 69–71, 73, 102, 141, 155, 157, 162] and uses Generative Dual Adversarial Network (GDAN) [25, 65, 75, 76, 93, 96, 142, 143, 150–152, 154, 156], overcomplete distributions [30, 38, 56, 77, 78, 83, 99, 100, 103, 105, 106, 130, 148, 149, 153, 164] and domain aware visual bias elimination [45–48, 52, 80, 111, 118, 124, 126–129, 136, 147, 159]. But it has not been well explored for medical images. One major reason being the availability of class attribute vectors for natural images that describe characteristics of seen and unseen classes, but are challenging to obtain for medical images. Self-supervised learning (SSL) also addresses labeled data shortage and has found wide use in medical image analysis by using innovative pre-text tasks for active learning [33, 35, 62, 63, 104, 107, 110, 114–117, 119, 120, 122, 132, 135], anomaly detection [8, 10, 11, 20, 26, 27, 36, 59–61, 67, 72, 74, 92, 112, 146], and data augmentation [3–5, 57, 64, 66, 71, 84, 85, 87–91]. SSL has been applied to histopathology images using domain specific pretext tasks [1, 18, 23, 32, 86, 95, 108, 113, 144], semi-supervised histology classification [42], stain normalization [73], registration [157] and cancer subtyping using visual dictionaries. Wu et al. [160] combine SSL and GZSL for natural images but rely on class attribute vectors and unlabeled target data for training.

Our current work makes the following contributions: 1) We propose a **multi-modal framework for seen and unseen Gleason grade prediction from MR images by combining GZSL and SSL**. 2) Unlike previous methods used for natural images we do not require class attribute vectors nor unlabeled target data during training. 3) We propose a **self-supervised learning (SSL)** approach for feature synthesis of seen and unseen classes that exploits the ordered relationship between different Gleason grades to generate new features. Although the method by [6] uses features from MRI and histopathology images: 1) it is a fully supervised method that has no Unseen classes during test time; 2) it also uses MRI and histopathology features from available data while we generate synthetic features to overcome unavailability of one data modality.

## 2 Method

### 2.1 Feature Extraction And Transformation:

Figure 1 depicts our overall proposed workflow, which has 3 networks for: feature extraction, feature transformation and self supervised feature synthesis. Let the training set consist of *histopathology and MR images* from PCa cases with known Gleason grades. We train a network that can correctly predict seen and unseen Gleason grades using *MR images only*. Let the dataset of ‘Seen’ and ‘Unseen’ classes be  $S, U$  and their corresponding labels be  $\mathcal{Y}_s, \mathcal{Y}_u$ .  $\mathcal{Y} = \mathcal{Y}_s \cup \mathcal{Y}_u$ , and  $\mathcal{Y}_s \cap \mathcal{Y}_u = \emptyset$ . Previous works [16] show that generating feature vectors, instead of images, performs better for GZSL classification since output images of generative models can be blurry, especially with multiple objects (e.g., multiple cells

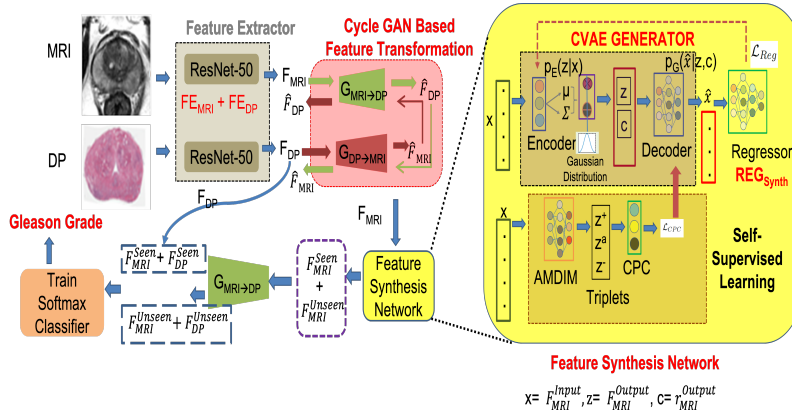


Fig. 1: **Training Workflow:** Feature extraction from MR and digital pathology images generates respective feature vectors  $F_{MRI}$  and  $F_{DP}$ . A  $F_{MRI}$  is input to a feature synthesis network to generate new MR features for ‘Seen’ and ‘Unseen’ classes, which are passed through the feature transformation network to obtain corresponding  $F_{DP}$ . Combined MR and histopathology features are used to train a softmax classifier for identifying ‘Seen’ and ‘Unseen’ test classes. A self-supervised module contributes to the sample generation step through  $\mathcal{L}_{CPC}$ .

in histopathology images). Additionally, generating high-resolution histopathology images from low resolution and noisy MRI is challenging, while finding a transformation between their feature vectors is much more feasible.

We train two separate ResNet-50 networks [22] as feature extractors for MR and DP images. Histopathology image feature extractor ( $FE_{DP}$ ) is pre-trained on the PANDA dataset [14] that has a large number of whole slide images for PCa classification.  $FE_{MRI}$  is pre-trained with the PROMISE12 challenge dataset [40] in a self-supervised manner. Since PROMISE12 is for prostate segmentation from MRI and does not have classification labels, we use a pre-text task of predicting if an image slice has the prostate or not. Gleason grades of MRI are the same as corresponding histopathology images. The images are processed through the convolution blocks and the 1000 dimensional output of the last FC layer is the feature vector for MRI ( $F_{MRI}$ ) and pathology images ( $F_{DP}$ ).

**Feature Transformation** is achieved using CycleGANs [65, 93, 94, 96, 163] to learn mapping functions  $G : X \rightarrow Y$  and  $F : Y \rightarrow X$ , between feature vectors  $X = F_{MRI}$  and  $Y = F_{DP}$ . Adversarial discriminator  $D_X$  differentiates between real features  $F_{DP}$  and generated features  $\hat{F}_{DP}$ , and  $D_Y$  distinguishes between  $F_{MRI}$  and  $\hat{F}_{MRI}$ . The adversarial loss (Eqn 1) and cycle consistency loss (Eqn. 2) are,

$$\begin{aligned}
 L_{adv}(G, D_Y) &= \mathbb{E}_y [\log D_Y(y)] + \mathbb{E}_x [\log (1 - D_Y(G(x)))] , \\
 L_{adv}(F, D_X) &= \mathbb{E}_x [\log D_X(x)] + \mathbb{E}_y [\log (1 - D_X(F(y)))] .
 \end{aligned}
 \tag{1}$$

$$L_{cyc}(G, F) = E_x \|F(G(x)) - x\|_1 + E_y \|G(F(y)) - y\|_1. \quad (2)$$

**Network Training** : is done using  $L_{adv}(G, D_Y) + L_{adv}(F, D_X) + L_{cyc}(G, F)$ . Generator  $G$  is a multi-layer perceptron (MLP) with a hidden layer of 4096 nodes having LeakyReLU [43]. The output layer with 2048 nodes has ReLU activation [138].  $G$ 's weights are initialized with a truncated normal of  $\mu = 0$ ,  $\sigma = 0.01$ , and biases initialized to 0. Discriminator  $D$  is an MLP with a hidden layer of 2048 nodes activated by LeakyReLU, and the output layer has no activation.  $D$ 's initialization is the same as  $G$ , and we use Adam optimizer [31].

## 2.2 CVAE Based Feature Generator Using Self Supervision

The conditional variational autoencoder (CVAE) generator synthesizes feature vectors  $F_{MRI}^{output}$  of desired class  $c_{MRI}^{output}$ , given input features  $F_{MRI}^{input}$  with known class  $c_{MRI}^{input}$ . Let  $x = F_{MRI}^{input}$ ,  $z = F_{MRI}^{output}$  and  $c = c_{MRI}^{output}$ . The CVAE loss is,

$$\min_{\theta_G, \theta_E} \mathcal{L}_{CVAE} + \lambda_c \cdot \mathcal{L}_c + \lambda_{reg} \cdot \mathcal{L}_{reg} + \lambda_E \cdot \mathcal{L}_E + \lambda_{CPC} \cdot \mathcal{L}_{CPC} \quad (3)$$

Denoting CVAE encoder as  $p_E(z|x)$  with parameters  $\theta_E$ , and the regressor output distribution as  $p_R(c|x)$ ,  $\mathcal{L}_{CVAE}$  is:

$$\mathcal{L}_{CVAE}(\theta_E, \theta_G) = -\mathbb{E}_{p_E(z|x), p(c|x)} [\log p_G(x|z, c)] + KL(p_E(z|x)||p(z)) \quad (4)$$

$\mathbb{E}_{p_E(z|x), p(c|x)}(\cdot)$  is the generator's reconstruction error, and KL divergence,  $KL(\cdot)$ , encourages CVAE posterior (the encoder) to be close to the prior. Encoder  $p_E(z|x)$ , conditional decoder/generator  $p_G(x|z, c)$ , and regressor  $p_R(c|x)$  are modeled as Gaussian distributions. The latent code  $(z, c)$  is represented by disentangled representations  $p_E(z|x)$  and  $p_R(c|x)$  to avoid posterior collapse [24].

**Regression/Discriminator Module -  $REG_{Synth}$** : is a feedforward neural network mapping input feature vector  $x \in \mathcal{R}^D$  to its corresponding class-value  $c \in \mathcal{R}^1$ .  $REG_{Synth}$  is a probabilistic model  $p_R(c|x)$  with parameters  $\theta_R$  and is trained using supervised ( $\mathcal{L}_{Sup}$ ) and unsupervised ( $\mathcal{L}_{Unsup}$ ) losses:

$$\min_{\theta_R} \mathcal{L}_R = \mathcal{L}_{Sup} + \lambda_R \cdot \mathcal{L}_{Unsup} \quad (5)$$

$\lambda_R = 0.2$  and  $\mathcal{L}_{Sup}(\theta_R) = -\mathbb{E}_{\{x_n, c_n\}} [p_R(c_n|x_n)]$  is defined on labeled examples  $\{x_n, c_n\}_{n=1}^N$  from the seen class.  $\mathcal{L}_{Unsup}(\theta_R) = -\mathbb{E}_{p_{\theta_G}(\hat{x}|z, c)p(z)p(c)} [p_R(c|\hat{x})]$  is defined on synthesized examples  $\hat{x}$  from the generator.  $\mathcal{L}_{Unsup}$  is obtained by sampling  $z$  from  $p(z)$ , and class-value  $c$  sampled from  $p(c)$  to generate an exemplar for  $p_{\theta_G}(\hat{x}|z, c)$ , and we calculate the expectation w.r.t. these distributions.

**Discriminator-Driven Learning**: The error back-propagated from  $REG_{Synth}$  improves quality of synthetic samples  $\hat{x}$  making them similar to the desired output class-value  $c$ . This is achieved using multiple loss functions. The first generates samples whose regressed class value is close to the desired value,

$$\mathcal{L}_c(\theta_G) = -\mathbb{E}_{p_G(\hat{x}|z, c)p(z)p(c)} [\log p_R(c|\hat{x})] \quad (6)$$

The second term draws samples from prior  $p(z)$  and combines with class-value from  $p(c)$ , to ensure the synthesized features are similar to the training data,

$$\mathcal{L}_{Reg}(\theta_G) = -\mathbb{E}_{p(z)p(c)} [\log p_G(\hat{x}|z, c)] \quad (7)$$

The third loss term ensures independence (disentanglement) [24] of  $z$  from the class-value  $c$ . The encoder ensures that the sampling distribution and the one obtained from the generated sample follow the same distribution.

$$\mathcal{L}_E(\theta_G) = -\mathbb{E}_{\hat{x} \sim p_G(\hat{x}|z, c)} KL [\log p_E(z|\hat{x}) || q(z)] \quad (8)$$

The distribution  $q(z)$  could be the prior  $p(z)$  or the posterior from a labeled sample  $p(z|x_n)$ .

**Self Supervised Loss:** Gleason grades have a certain ordering, i.e., grade 3 indicates higher severity than grade 1, and grade 5 is higher than grade 3. Contrastive Predictive Coding (CPC) [140] learns self-supervised representations by predicting future observations from past ones and requires that observations be ordered in some dimension. Inspired by CPC we train our network to predict features of desired Gleason grade from input features of a different grade. From the training data we construct pairs of  $\{F_{MRI}^{input}, c_{MRI}^{input}, F_{MRI}^{output}, c_{MRI}^{output}\}$ , the input and output features and desired class label value  $c_{MRI}^{output}$  of synthesized vector.

Since the semantic gap between  $F_{MRI}^{input}$  and  $F_{MRI}^{output}$  may be too large, we use random transformations to first generate intermediate representation of positive  $z^+$ , anchor  $z^a$  and negative  $z^-$  features using the mutual information-based AMDIM approach of [2]. AMDIM ensures that the mutual information between similar samples  $z^+, z^a$  is high while for dissimilar samples  $z^-, z^a$  it is low, where  $z = F_{MRI}^{output}$ . The CPC objective (Eqn. 9) evaluates the quality of the predictions using a contrastive loss where the goal is to correctly recognize the synthetic vector  $z$  among a set of randomly sampled feature vectors  $z_l = \{z^+, z^a, z^-\}$ .

$$\mathcal{L}_{CPC} = - \sum \log \frac{\exp^{(F_{MRI}^{input})^T F_{MRI}^{output}}}{\exp^{(F_{MRI}^{input})^T F_{MRI}^{output}} + \sum \exp^{(F_{MRI}^{input})^T F_{MRI}^{output}}} \quad (9)$$

This loss is the InfoNCE inspired from Noise-Contrastive Estimation [21, 137] and maximizes the mutual information between  $c$  and  $z$  [140]. By specifying the desired class label value of synthesized vector and using it to guide feature generation in the CVAE framework we avoid the pitfalls of unconstrained and unrealistic feature generation common in generative model based GZSL (e.g., [41, 161]).

**Training And Implementation:** Our framework was implemented in PyTorch. The CVAE Encoder has two hidden layers of 2000 and 1000 units respectively while the CVAE Generator is implemented with one hidden layer of 1000 hidden units. The Regressor has only one hidden layer of 800 units. We choose Adam [31] as our optimizer, and the momentum is set to (0.9, 0.999). The learning rate for CVAE and Regressor is 0.0001. First the CVAE loss (Eqn. 4) is

pre-trained followed by joint training of regressor and encoder-generator pair in optimizing Eqn. 7 and Eqn. 3 till convergence. Hyperparameter values were chosen using a train-validation split with  $\lambda_R = 0.1$ ,  $\lambda_c = 0.1$ ,  $\lambda_{reg} = 0.1$ ,  $\lambda_E = 0.1$ , and  $\lambda_{CPC} = 0.2$ . Training the feature extractor for 50 epochs takes 12 hours and the feature synthesis network for 50 epochs takes 17 hours, all on a single NVIDIA V100 GPU (32 GB RAM).

**Evaluation Protocol:** The seen class  $S$  has samples from 2 or more Gleason grades, and the unseen class  $U$  contains samples from remaining classes. 80 – 20 split of  $S$  is done into  $S_{Train}/S_{Test}$ .  $F_{MRI}$  is synthesized from  $S + U$  using the CVAE and combined with the corresponding synthetic  $F_{DP}$  to obtain a single feature vector for training a softmax classifier minimizing the negative log-likelihood loss. Following standard practice for GZSL, average class accuracies are calculated for two settings: 1) *Setting A*: training is performed on synthesized samples of  $S + U$  classes and test on  $S_{Test}$ . 2) *Setting B*: training is performed on synthesized samples of  $S + U$  classes and test on  $U$ . Following GZSL protocol we report the harmonic mean:  $H = \frac{2 \times Acc_U \times Acc_S}{Acc_U + Acc_S}$ ;  $Acc_S$  and  $Acc_U$  are classification accuracy of images from seen (setting A) and unseen (setting B) classes respectively:

### 3 Experimental Results

**Dataset Details:** We use images from 321 patients (48 – 70 years; mean: 58.5 years) undergone prostate surgery with pre-operative T2-w and Apparent Diffusion Coefficient MRI, and post-operative digitized histopathology images. To ensure prostate tissue is sectioned in same plane as T2w MRI custom 3D printed molds were used. Majority votes among three pathologists provided Gleason grades was the consensus annotation. Pre-operative MRI and histopathology images were registered [145] to enable accurate mapping of cancer labels. We have the following classes: Class 1 : *Grade – 3*, 67 patients, Class 2 : *Grades – 3 + 4/4 + 3*, 60 patients, Class 3 : *Grade – 4*, 74 patients, Class 4 : *Grades – 4 + 5/5 + 4*, 57 patients, Class 5 : *Grade – 5*, 63 patients. In the supplementary we show results for the Kaggle DR challenge [17] and PANDA challenge [14].

**Pre-processing:** Histopathology images were smoothed with a Gaussian filter ( $\sigma = 0.25$ ). They were downsampled to  $224 \times 224$  with X-Y resolution  $0.25 \times 0.25 \text{ mm}^2$ . The T2w images, prostate masks, and Gleason labels are projected on the corresponding downsampled histopathology images and resampled to the same X-Y resolution. This ensures corresponding pixels in each modality represents the same physical area. MR images were normalized using histogram alignment [139]. The training, validation, and test sets had 193/64/64 patients.

We compare results of our method  $MM_{GZSL}$  (Multimodal GZSL) with different feature generation based GZSL methods: 1) CVAE based feature synthesis method of [25]; 2) GZSL using over complete distributions [30]; 3) self-supervised learning GZSL method of [160]; 4) cycle-GAN GZSL method of [16]; 5) *FSL*- the

fully supervised learning method of [6] using the same data split, actual labels of ‘Unseen’ class and almost equal representation of all classes.

	$Acc_S$	$Acc_U$	H	p	$Sens$	$Spe_S$	$Sens_U$	$Spe_U$
<b>Comparison Methods</b>								
MM $_{GZSL}$	83.6(2.4)	81.7(3.0)	82.6(2.8)	-	84.1(3.1)	82.9(2.6)	81.2(3.0)	80.1(3.3)
[25]	80.3(3.5)	73.4(3.6)	76.7(2.8)	0.002	81.2(3.6)	79.9(3.5)	74.1(3.2)	72.8(3.4)
[30]	80.6(3.4)	72.8(3.0)	76.5(3.2)	0.001	81.1(2.9)	80.0(3.2)	73.5(3.1)	72.1(3.4)
[160]	81.1(2.9)	73.2(3.2)	76.9(3.1)	0.001	81.8(3.5)	80.7(3.1)	74.0(3.5)	72.9(3.7)
[16]	81.2(3.7)	72.8(3.8)	76.7(3.8)	0.004	81.8(3.1)	80.7(3.4)	73.1(4.0)	71.9(4.2)
FSL	83.9(2.2)	83.3(2.5)	83.5(2.3)	0.01	84.9(2.4)	83.5(2.6)	83.7(2.8)	82.5(2.6)
<b>Ablation Studies</b>								
MM $_{wCPC}$	79.1(3.1)	72.3(3.8)	75.5(3.4)	0.001	79.8(3.4)	78.3(3.5)	73(3.6)	82.5(3.1)
MM $_{wReg}$	80.1(3.7)	72.2(3.5)	75.9(3.5)	0.0001	80.5(3.4)	78.8(3.5)	72.8(3.8)	71.3(4.0)
MM $_{wC}$	79.2(3.9)	72.9(4.0)	75.9(3.9)	0.009	80.1(3.8)	78.6(4.3)	73.3(4.1)	72.1(4.2)
MM $_{wE}$	80.2(3.7)	73.0(3.9)	76.4(3.7)	0.005	80.8(3.3)	79.5(3.8)	74.1(3.8)	72.4(3.4)
MM $_{MR}$	75.6(4.2)	71.1(4.5)	73.3(4.3)	0.007	76.3(4.5)	75.0(4.3)	71.9(4.1)	70.4(4.3)
MM $_{DP}$	81.2(3.0)	79.1(3.6)	80.1(3.4)	0.008	82.0(3.4)	80.6(3.5)	79.9(3.9)	78.4(4.2)

Table 1: **GZSL and Ablation Results:** Average classification accuracy (%) and harmonic mean accuracy of generalized zero-shot learning when test samples are from Seen (Setting  $A$ ) or unseen (Setting  $B$ ) classes. Mean and variance are reported when the number of classes in the ‘Seen’ set is 3.  $p$  values are with respect to **Harmonic Mean of MM $_{GZSL}$** .

### 3.1 Generalized Zero Shot Learning Results

Table 1 summarizes the results of our algorithm and other methods when the Seen set has samples from 3 classes. The numbers are an average of 5 runs. Samples from 3 labeled classes presents the optimum scenario balancing high classification accuracy, and generation of representative synthetic samples. Setting  $A$  does better than setting  $B$ . Since GZSL is a very challenging problem, it is expected that classification performance on Unseen classes will not match those of Seen classes. MM $_{GZSL}$ ’s performance is closest to FSL. Since FSL has been trained with all classes in training and test sets it gives the best results.

We use the McNemar test and determine that the difference in  $Acc_S$  of MM $_{GZSL}$  and FSL is not significant ( $p = 0.062$ ) although the corresponding values for  $Acc_U$  are significant ( $p = 0.031$ ) which is not surprising since real Unseen examples have not been encountered in GZSL. Since MM $_{GZSL}$ ’s performance is closest to FSL for Unseen classes, it demonstrates MM $_{GZSL}$ ’s effectiveness in generating realistic features of unseen classes. We refer the reader to the supplementary material for additional results (e.g. using different number of classes in the Seen dataset). The individual Per Class mean accuracy and

variance are: **Setting A**:-Class1=84.1(2.4), Class2=83.8(2.8), Class3=84.1(2.3), Class4=82.9(2.8), Class5=82.9(3.1). **Setting B**- Class1=83.1(2.7), Class2=82.9(2.8), Class3=81.1(2.9), Class4=79.0(3.2), Class5=78.2(3.9). This shows that our feature generation and classification is not biased to any specific class.

**Ablation Studies:** Table 1 shows ablation results where each row denotes a specific setting without the particular term in the final objective function in Eqn 3 - e.g.,  $MM_{wCPC}$  denotes our proposed method  $MM_{GZSL}$  without the self-supervised loss  $\mathcal{L}_{CPC}$ .  $MM_{wCPC}$  shows the worst performance indicating  $\mathcal{L}_{CPC}$ 's correspondingly higher contribution than other terms. The  $p$ -values indicate each term's contribution is significant for the overall performance of  $MM_{GZSL}$  and excluding any one leads to significant performance degradation.

We also show in Table 1 the result of using: 1) only the synthetic MR features ( $MM_{MR}$ ); 2) only digital histopathology features ( $MM_{DP}$ ) obtained by transforming  $F_{MRI}$  to get  $F_{DP}$ .  $MM_{DP}$  gives performance metrics closer to  $MM_{GZSL}$ , which indicates that the digital histopathology images provide highly discriminative information compared to MR images. However, MR images also have a notable contribution, as indicated by the  $p$ -values. In another set of experiments we redesign the GZSL experiments to generate synthetic histopathology features  $F_{DP}$  instead of  $F_{MRI}$  and then transforming them to get MR features. We obtain very similar performance ( $Acc_S = 83.7, Acc_U = 80.8, H = 82.2$ ) to the original  $MM_{GZSL}$  setting. This demonstrates that cycle GAN based feature transformation network does a good job of learning accurate histopathology features from the corresponding MR features.

**Visualization of Synthetic Features :** Figure 2 (a) shows t-SNE plot of real data features where the classes are spread over a wide area, with overlap amongst consecutive classes. Figures 2 (b,c,d) show, respectively, distribution of synthetic features generated by  $MM_{GZSL}$ ,  $MM_{wCPC}$  and [160].  $MM_{GZSL}$  features are the most similar to the original data.  $MM_{wCPC}$  and [160] synthesize sub-optimal feature representation of actual features, resulting in poor classification performance on unseen classes.

## 4 Conclusion

We propose a GZSL approach without relying on class attribute vectors. Our novel method can accurately predict Gleason grades from MR images with lower resolution and less information content than histopathology images. This has the potential to improve accuracy of early detection and staging of PCa. A self-supervised component ensures the semantic gap between Seen and Unseen classes is easily covered. The distribution of synthetic features generated by our method are close to the actual distribution, while removing the self-supervised term results in unrealistic distributions. Results show our method's superior performance and synergy between different loss terms leads to improved GZSL



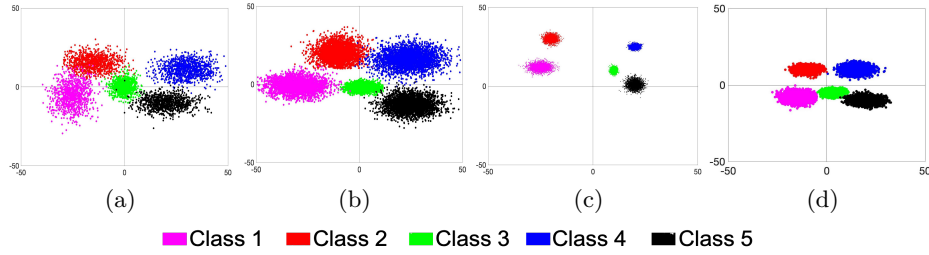


Fig. 2: Feature visualizations: (a) Seen+Unseen classes from actual dataset; distribution of synthetic samples generated by b)  $MM_{GZSL}$ ; (c)  $MM_{GZSL}$  without self-supervision; (d) for [160]. Different colours represent different classes. (b) is closer to (a), while (c) and (d) are quite different.

classification. We observe failure cases where the acquired MR images are not of sufficiently good resolution to allow accurate registration of histopathology and MRI. Future work will aim to address this issue.

## References

1. Antony, B., Sedai, S., Mahapatra, D., Garnavi, R.: Real-time passive monitoring and assessment of pediatric eye health. In: US Patent App. 16/178,757 (2020)
2. Bachman, P., Hjelm, R.D., Buchwalter, W.: Learning representations by maximizing mutual information across views. In: In Proc. NeurIPS. pp. 15509–15519 (2019)
3. Bastide, P., Kiral-Kornek, I., Mahapatra, D., Saha, S., Vishwanath, A., Cavallar, S.V.: Machine learned optimizing of health activity for participants during meeting times. In: US Patent App. 15/426,634 (2018)
4. Bastide, P., Kiral-Kornek, I., Mahapatra, D., Saha, S., Vishwanath, A., Cavallar, S.V.: Visual health maintenance and improvement. In: US Patent 9,993,385 (2018)
5. Bastide, P., Kiral-Kornek, I., Mahapatra, D., Saha, S., Vishwanath, A., Cavallar, S.V.: Crowdsourcing health improvements routes. In: US Patent App. 15/611,519 (2019)
6. Bhattacharya, I., Seetharaman, A., Shao, W., Sood, R., Kunder, C.A., et al.: Corrsignet: Learning correlated prostate cancer signatures from radiology and pathology images for improved computer aided diagnosis. In: In Proc MICCAI. pp. 315–325 (2020)
7. Bozorgtabar, B., Mahapatra, D., von Teng, H., Pollinger, A., Ebner, L., Thiran, J.P., Reyes, M.: Informative sample generation using class aware generative adversarial networks for classification of chest xrays. *Computer Vision and Image Understanding* **184**, 57–65 (2019)
8. Bozorgtabar, B., Mahapatra, D., von Teng, H., Pollinger, A., Ebner, L., Thiran, J.P., Reyes, M.: Informative sample generation using class aware generative adversarial networks for classification of chest xrays. In: arXiv preprint arXiv:1904.10781 (2019)

9. Bozorgtabar, B., Mahapatra, D., Thiran, J.P.: Exprada: Adversarial domain adaptation for facial expression analysis. In *Press Pattern Recognition* **100**, 15–28 (2020)
10. Bozorgtabar, B., Mahapatra, D., Thiran, J.P., Shao, L.: SALAD: Self-supervised aggregation learning for anomaly detection on x-rays. In: *In Proc. MICCAI*. pp. 468–478 (2020)
11. Bozorgtabar, B., Mahapatra, D., Vray, G., Thiran, J.P.: Anomaly detection on x-rays using self-supervised aggregation learning. In: *arXiv preprint arXiv:2010.09856* (2020)
12. Bozorgtabar, B., Mahapatra, D., Zlobec, I., Rau, T., Thiran, J.: Computational pathology. *Frontiers in Medicine* **7** (2020)
13. Bozorgtabar, B., Rad, M.S., Mahapatra, D., Thiran, J.P.: Syndemo: Synergistic deep feature alignment for joint learning of depth and ego-motion. In: *In Proc. IEEE ICCV* (2019)
14. Bulten, W., Pinckaers, H., van Boven, H., Vink, R., de Bel, T., van Ginneken, B., van der Laak, J., van de Kaa, C.H., Litjens, G.: Automated deep-learning system for gleason grading of prostate cancer using biopsies: a diagnostic study. *Lancet Oncology* **21**(2), 233–241 (2020)
15. Campanella, G., Silva, V.M., Fuchs, T.J.: Terabyte-scale deep multiple instance learning for classification and localization in pathology. In: *arXiv preprint arXiv:1805.06983* (2018)
16. Felix, R., Kumar, V., Reid, I., Carneiro, G.: Multi-modal cycle-consistent generalized zero-shot learning. In: *ECCV*. pp. 21–37 (2018)
17. Foundation, C.H.: Diabetic retinopathy detection. [online]. available: <https://www.kaggle.com/c/diabetic-retinopathy-detection>
18. Garnavi, R., Mahapatra, D., Roy, P., Tennakoon, R.: System and method to teach and evaluate image grading performance using prior learned expert knowledge base. In: *US Patent App. 10,657,838* (2020)
19. Ge, Z., Mahapatra, D., Chang, X., Chen, Z., Chi, L., Lu, H.: Improving multi-label chest x-ray disease diagnosis by exploiting disease and health labels dependencies. In *press Multimedia Tools and Application* pp. 1–14 (2019)
20. Ge, Z., Mahapatra, D., Sedai, S., Garnavi, R., Chakravorty, R.: Chest x-rays classification: A multi-label and fine-grained problem. In: *arXiv preprint arXiv:1807.07247* (2018)
21. Gutmann, M., Hyvarinen, A.: A new estimation principle for unnormalized statistical models. In: *In Proc. AISTATS*. pp. 297–304 (2010)
22. He, K., Zhang, X., Ren, S., Sun, J.: Deep residual learning for image recognition. In: *In Proc. CVPR*. pp. 770–778 (2016)
23. Hoog, J.D., Mahapatra, D., Garnavi, R., Jalali, F.: Personalized monitoring of injury rehabilitation through mobile device imaging. In: *US Patent App. 16/589,046* (2021)
24. Hu, Z., Yang, Z., Liang, X., Salakhutdinov, R., Xing, E.P.: Toward controlled generation of text. In: *In Proc. ICML*. pp. 1587–1596 (2017)
25. Huang, H., Wang, C., Yu, P.S., Wang, C.D.: Generative dual adversarial network for generalized zero-shot learning. In: *The IEEE Conference on Computer Vision and Pattern Recognition (CVPR)*. pp. 801–810 (June 2019)
26. Ju, L., Wang, X., Wang, L., Liu, T., Zhao, X., Drummond, T., Mahapatra, D., Ge, Z.: Relational subsets knowledge distillation for long-tailed retinal diseases recognition. In: *arXiv preprint arXiv:2104.11057* (2021)

27. Ju, L., Wang, X., Wang, L., Mahapatra, D., Zhao, X., Harandi, M., Drummond, T., Liu, T., Ge, Z.: Improving medical image classification with label noise using dual-uncertainty estimation. In: arXiv preprint arXiv:2103.00528 (2020)
28. Ju, L., Wang, X., Zhao, X., Lu, H., Mahapatra, D., Bonnington, P., Ge, Z.: Synergic adversarial label learning for grading retinal diseases via knowledge distillation and multi-task learning. *IEEE JBHI* **100**, 1–14 (2020)
29. Ju, L., Wang, X., Zhao, X., Lu, H., Mahapatra, D., Ge, Z.: Relational subsets knowledge distillation for long-tailed retinal diseases recognition. In: In MICCAI 2021. pp. 1–11 (2021)
30. Keshari, R., Singh, R., Vatsa, M.: Generalized zero-shot learning via over-complete distribution. In: The IEEE Conference on Computer Vision and Pattern Recognition (CVPR). pp. 13300–13308 (June 2020)
31. Kingma, D.P., Ba, J.: Adam: A method for stochastic optimization. In: arXiv preprint arXiv:1412.6980, (2014)
32. Koozbanani, N.A., Unnikrishnan, B., Khurram, S.A., Krishnaswamy, P., Rajpoot, N.: Self-path: Self-supervision for classification of pathology images with limited annotations. In: arXiv:2008.05571 (2020)
33. Kuanar, S., Athitsos, V., Mahapatra, D., Rajan, A.: Multi-scale deep learning architecture for nucleus detection in renal cell carcinoma microscopy image. In: arXiv preprint arXiv:2104.13557 (2021)
34. Kuanar, S., Athitsos, V., Mahapatra, D., Rao, K., Akhtar, Z., Dasgupta, D.: Low dose abdominal ct image reconstruction: An unsupervised learning based approach. In: In Proc. IEEE ICIP. pp. 1351–1355 (2019)
35. Kuanar, S., Mahapatra, D., Athitsos, V., Rao, K.: Gated fusion network for sao filter and inter frame prediction in versatile video coding. In: arXiv preprint arXiv:2105.12229 (2021)
36. Kuanar, S., Rao, K., Mahapatra, D., Bilas, M.: Night time haze and glow removal using deep dilated convolutional network. In: arXiv preprint arXiv:1902.00855 (2019)
37. Kuanar, S., Mahapatra, D., Bilas, M., Rao, K.: Multi-path dilated convolution network for haze and glow removal in night time images. *The Visual Computer* pp. 1–14 (2021)
38. Kuang, H., Guthier, B., Saini, M., Mahapatra, D., Saddik, A.E.: A real-time smart assistant for video surveillance through handheld devices. In: In Proc. ACM Intl. Conf. Multimedia. pp. 917–920 (2014)
39. Li, Z., Mahapatra, D., J.Tielbeek, Stoker, J., van Vliet, L., Vos, F.: Image registration based on autocorrelation of local structure. *IEEE Trans. Med. Imaging* **35**(1), 63–75 (2016)
40. Litjens, G., Toth, R., de Ven, W., Hoeks, C., et al: Evaluation of prostate segmentation algorithms for mri: The PROMISE12 challenge. *Medical Image Analysis* **18**(2), 359–373 (2014)
41. Long, Y., Liu, L., Shen, F., Shao, L., Li, X.: Zero-shot learning using synthesised unseen visual data with diffusion regularisation. *IEEE Trans. Pattern Analysis Machine Intelligence* **40**(10), 2498 – 2512 (2017)
42. Lu, M.Y., Chen, R.J., Wang, J., Dillon, D., Mahmood, F.: Semi-supervised histology classification using deep multiple instance learning and contrastive predictive coding. In: arXiv:1910.10825 (2019)
43. Maas, A.L., Hannun, A.Y., Ng, A.Y.: Rectifier nonlinearities improve neural network acoustic models. In: In Proc. ICML (2013)

44. Mahapatra, D.: Elastic registration of cardiac perfusion images using saliency information. *Sequence and Genome Analysis – Methods and Applications* pp. 351–364 (2011)
45. Mahapatra, D.: Neonatal brain mri skull stripping using graph cuts and shape priors. In: *In Proc: MICCAI workshop on Image Analysis of Human Brain Development (IAHBD)* (2011)
46. Mahapatra, D.: Cardiac lv and rv segmentation using mutual context information. In: *Proc. MICCAI-MLMI*. pp. 201–209 (2012)
47. Mahapatra, D.: Groupwise registration of dynamic cardiac perfusion images using temporal information and segmentation information. In: *In Proc: SPIE Medical Imaging* (2012)
48. Mahapatra, D.: Landmark detection in cardiac mri using learned local image statistics. In: *Proc. MICCAI-Statistical Atlases and Computational Models of the Heart. Imaging and Modelling Challenges (STACOM)*. pp. 115–124 (2012)
49. Mahapatra, D.: Skull stripping of neonatal brain mri: Using prior shape information with graphcuts. *J. Digit. Imaging* **25**(6), 802–814 (2012)
50. Mahapatra, D.: Cardiac image segmentation from cine cardiac mri using graph cuts and shape priors. *J. Digit. Imaging* **26**(4), 721–730 (2013)
51. Mahapatra, D.: Cardiac mri segmentation using mutual context information from left and right ventricle. *J. Digit. Imaging* **26**(5), 898–908 (2013)
52. Mahapatra, D.: Graph cut based automatic prostate segmentation using learned semantic information. In: *Proc. IEEE ISBI*. pp. 1304–1307 (2013)
53. Mahapatra, D.: Joint segmentation and groupwise registration of cardiac perfusion images using temporal information. *J. Digit. Imaging* **26**(2), 173–182 (2013)
54. Mahapatra, D.: An automated approach to cardiac rv segmentation from mri using learned semantic information and graph cuts. *J. Digit. Imaging*. **27**(6), 794–804 (2014)
55. Mahapatra, D.: Combining multiple expert annotations using semi-supervised learning and graph cuts for medical image segmentation. *Computer Vision and Image Understanding* **151**(1), 114–123 (2016)
56. Mahapatra, D.: Retinal image quality classification using neurobiological models of the human visual system. In: *In Proc. MICCAI-OMIA*. pp. 1–8 (2016)
57. Mahapatra, D.: Consensus based medical image segmentation using semi-supervised learning and graph cuts. In: *arXiv preprint arXiv:1612.02166* (2017)
58. Mahapatra, D.: Semi-supervised learning and graph cuts for consensus based medical image segmentation. *Pattern Recognition* **63**(1), 700–709 (2017)
59. Mahapatra, D.: Amd severity prediction and explainability using image registration and deep embedded clustering. In: *arXiv preprint arXiv:1907.03075* (2019)
60. Mahapatra, D.: Generative adversarial networks and domain adaptation for training data independent image registration. In: *arXiv preprint arXiv:1910.08593* (2019)
61. Mahapatra, D.: Registration of histopathogy images using structural information from fine grained feature maps. In: *arXiv preprint arXiv:2007.02078* (2020)
62. Mahapatra, D.: Interpretability-driven sample selection using self supervised learning for disease classification and segmentation. In: *arXiv preprint arXiv:2104.06087* (2021)
63. Mahapatra, D.: Learning of inter-label geometric relationships using self-supervised learning: Application to gleason grade segmentation. In: *arXiv preprint arXiv:2110.00404* (2021)

64. Mahapatra, D., Agarwal, K., Khosrowabadi, R., Prasad, D.: Recent advances in statistical data and signal analysis: Application to real world diagnostics from medical and biological signals. In: Computational and mathematical methods in medicine (2016)
65. Mahapatra, D., Antony, B., Sedai, S., Garnavi, R.: Deformable medical image registration using generative adversarial networks. In: In Proc. IEEE ISBI. pp. 1449–1453 (2018)
66. Mahapatra, D., Bozorgtabar, B.: Retinal vasculature segmentation using local saliency maps and generative adversarial networks for image super resolution. In: arXiv preprint arXiv:1710.04783 (2017)
67. Mahapatra, D., Bozorgtabar, B.: Progressive generative adversarial networks for medical image super resolution. In: arXiv preprint arXiv:1902.02144 (2019)
68. Mahapatra, D., Bozorgtabar, B., Garnavi, R.: Image super-resolution using progressive generative adversarial networks for medical image analysis. *Computerized Medical Imaging and Graphics* **71**, 30–39 (2019)
69. Mahapatra, D., Bozorgtabar, B., Ge, Z.: Medical image classification using generalized zero shot learning. In: In IEEE CVAMD 2021. pp. 3344–3353 (2021)
70. Mahapatra, D., Bozorgtabar, B., Kuanar, S., Ge, Z.: Self-supervised multimodal generalized zero shot learning for gleason grading. In: In MICCAI-DART 2021. pp. 1–11 (2021)
71. Mahapatra, D., Bozorgtabar, B., Shao, L.: Pathological retinal region segmentation from oct images using geometric relation based augmentation. In: In Proc. IEEE CVPR. pp. 9611–9620 (2020)
72. Mahapatra, D., Bozorgtabar, B., Thiran, J.P., Shao, L.: Pathological retinal region segmentation from oct images using geometric relation based augmentation. In: arXiv preprint arXiv:2003.14119 (2020)
73. Mahapatra, D., Bozorgtabar, B., Thiran, J.P., Shao, L.: Structure preserving stain normalization of histopathology images using self supervised semantic guidance. In: In Proc. MICCAI. pp. 309–319 (2020)
74. Mahapatra, D., Bozorgtabar, B., Thiran, J.P., Shao, L.: Structure preserving stain normalization of histopathology images using self supervised semantic guidance. In: arXiv preprint arXiv:2008.02101 (2020)
75. Mahapatra, D., Bozorgtabar, S., Hewavitahranage, S., Garnavi, R.: Image super resolution using generative adversarial networks and local saliency maps for retinal image analysis. In: In Proc. MICCAI. pp. 382–390 (2017)
76. Mahapatra, D., Bozorgtabar, S., Thiran, J.P., Reyes, M.: Efficient active learning for image classification and segmentation using a sample selection and conditional generative adversarial network. In: In Proc. MICCAI (2). pp. 580–588 (2018)
77. Mahapatra, D., Buhmann, J.: Obtaining consensus annotations for retinal image segmentation using random forest and graph cuts. In: In Proc. OMIA. pp. 41–48 (2015)
78. Mahapatra, D., Buhmann, J.: Visual saliency based active learning for prostate mri segmentation. In: In Proc. MLMI. pp. 9–16 (2015)
79. Mahapatra, D., Buhmann, J.: Visual saliency based active learning for prostate mri segmentation. *SPIE Journal of Medical Imaging* **3**(1) (2016)
80. Mahapatra, D., Buhmann, J.: Automatic cardiac rv segmentation using semantic information with graph cuts. In: Proc. IEEE ISBI. pp. 1094–1097 (2013)
81. Mahapatra, D., Buhmann, J.: Analyzing training information from random forests for improved image segmentation. *IEEE Trans. Imag. Proc.* **23**(4), 1504–1512 (2014)

82. Mahapatra, D., Buhmann, J.: Prostate mri segmentation using learned semantic knowledge and graph cuts. *IEEE Trans. Biomed. Engg.* **61**(3), 756–764 (2014)
83. Mahapatra, D., Buhmann, J.: A field of experts model for optic cup and disc segmentation from retinal fundus images. In: *In Proc. IEEE ISBI*. pp. 218–221 (2015)
84. Mahapatra, D., Garnavi, R., Roy, P., Tennakoon, R.: System and method to teach and evaluate image grading performance using prior learned expert knowledge base. In: *US Patent App. 15/459,457* (2018)
85. Mahapatra, D., Garnavi, R., Roy, P., Tennakoon, R.: System and method to teach and evaluate image grading performance using prior learned expert knowledge base. In: *US Patent App. 15/814,590* (2018)
86. Mahapatra, D., Garnavi, R., Sedai, S., Roy, P.: Joint segmentation and characteristics estimation in medical images. In: *US Patent App. 15/234,426* (2017)
87. Mahapatra, D., Garnavi, R., Sedai, S., Roy, P.: Retinal image quality assessment, error identification and automatic quality correction. In: *US Patent 9,779,492* (2017)
88. Mahapatra, D., Garnavi, R., Sedai, S., Tennakoon, R.: Classification of severity of pathological condition using hybrid image representation. In: *US Patent App. 15/426,634* (2018)
89. Mahapatra, D., Garnavi, R., Sedai, S., Tennakoon, R.: Generating an enriched knowledge base from annotated images. In: *US Patent App. 15/429,735* (2018)
90. Mahapatra, D., Garnavi, R., Sedai, S., Tennakoon, R., Chakravorty, R.: Early prediction of age related macular degeneration by image reconstruction. In: *US Patent App. 15/854,984* (2018)
91. Mahapatra, D., Garnavi, R., Sedai, S., Tennakoon, R., Chakravorty, R.: Early prediction of age related macular degeneration by image reconstruction. In: *US Patent 9,943,225* (2018)
92. Mahapatra, D., Ge, Z.: Combining transfer learning and segmentation information with gans for training data independent image registration. In: *arXiv preprint arXiv:1903.10139* (2019)
93. Mahapatra, D., Ge, Z.: Training data independent image registration with gans using transfer learning and segmentation information. In: *In Proc. IEEE ISBI*. pp. 709–713 (2019)
94. Mahapatra, D., Ge, Z.: Training data independent image registration using generative adversarial networks and domain adaptation. *Pattern Recognition* **100**, 1–14 (2020)
95. Mahapatra, D., Ge, Z., Sedai, S.: Joint registration and segmentation of images using deep learning. In: *US Patent App. 16/001,566* (2019)
96. Mahapatra, D., Ge, Z., Sedai, S., Chakravorty, R.: Joint registration and segmentation of xray images using generative adversarial networks. In: *In Proc. MICCAI-MLMI*. pp. 73–80 (2018)
97. Mahapatra, D., Gilani, S., Saini, M.: Coherency based spatio-temporal saliency detection for video object segmentation. *IEEE Journal of Selected Topics in Signal Processing*. **8**(3), 454–462 (2014)
98. Mahapatra, D., J.Tielbeek, Makanyanga, J., Stoker, J., Taylor, S., Vos, F., Buhmann, J.: Automatic detection and segmentation of crohn’s disease tissues from abdominal mri. *IEEE Trans. Med. Imaging* **32**(12), 1232–1248 (2013)
99. Mahapatra, D., J.Tielbeek, Makanyanga, J., Stoker, J., Taylor, S., Vos, F., Buhmann, J.: Active learning based segmentation of crohn’s disease using principles of visual saliency. In: *Proc. IEEE ISBI*. pp. 226–229 (2014)

100. Mahapatra, D., J.Tielbeek, Makanyanga, J., Stoker, J., Taylor, S., Vos, F., Buhmann, J.: Combining multiple expert annotations using semi-supervised learning and graph cuts for crohn's disease segmentation. In: In Proc: MICCAI-ABD (2014)
101. Mahapatra, D., J.Tielbeek, Vos, F., Buhmann, J.: A supervised learning approach for crohn's disease detection using higher order image statistics and a novel shape asymmetry measure. *J. Digit. Imaging* **26**(5), 920–931 (2013)
102. Mahapatra, D., Kuanar, S., Bozorgtabar, B., Ge, Z.: Self-supervised learning of inter-label geometric relationships for gleason grade segmentation. In: In MICCAI-DART 2021. pp. 1–11 (2021)
103. Mahapatra, D., Li, Z., Vos, F., Buhmann, J.: Joint segmentation and groupwise registration of cardiac dce mri using sparse data representations. In: In Proc. IEEE ISBI. pp. 1312–1315 (2015)
104. Mahapatra, D., Routray, A., Mishra, C.: An active snake model for classification of extreme emotions. In: IEEE International Conference on Industrial Technology (ICIT). pp. 2195–2199 (2006)
105. Mahapatra, D., Roy, P., Sedai, S., Garnavi, R.: A cnn based neurobiology inspired approach for retinal image quality assessment. In: In Proc. EMBC. pp. 1304–1307 (2016)
106. Mahapatra, D., Roy, P., Sedai, S., Garnavi, R.: Retinal image quality classification using saliency maps and cnns. In: In Proc. MICCAI-MLMI. pp. 172–179 (2016)
107. Mahapatra, D., Roy, S., Sun, Y.: Retrieval of mr kidney images by incorporating shape information in histogram of low level features. In: In 13th International Conference on Biomedical Engineering. pp. 661–664 (2009)
108. Mahapatra, D., Saha, S., Vishwanath, A., Bastide, P.: Generating hyperspectral image database by machine learning and mapping of color images to hyperspectral domain. In: US Patent App. 15/949,528 (2019)
109. Mahapatra, D., Saini, M.: A particle filter framework for object tracking using visual-saliency information. *Intelligent Multimedia Surveillance* pp. 133–147 (2013)
110. Mahapatra, D., Saini, M., Sun, Y.: Illumination invariant tracking in office environments using neurobiology-saliency based particle filter. In: IEEE ICME. pp. 953–956 (2008)
111. Mahapatra, D., Schüffler, P., Tielbeek, J., Vos, F., Buhmann, J.: Semi-supervised and active learning for automatic segmentation of crohn's disease. In: Proc. MICCAI, Part 2. pp. 214–221 (2013)
112. Mahapatra, D., Sedai, S., Garnavi, R.: Elastic registration of medical images with gans. In: arXiv preprint arXiv:1805.02369 (2018)
113. Mahapatra, D., Sedai, S., Halupka, K.: Uncertainty region based image enhancement. In: US Patent App. 10,832,074 (2020)
114. Mahapatra, D., Singh, A.: Ct image synthesis using weakly supervised segmentation and geometric inter-label relations for covid image analysis. In: arXiv preprint arXiv:2106.10230 (2021)
115. Mahapatra, D., Sun, Y.: Nonrigid registration of dynamic renal MR images using a saliency based MRF model. In: Proc. MICCAI. pp. 771–779 (2008)
116. Mahapatra, D., Sun, Y.: Registration of dynamic renal mr images using neurobiological model of saliency. In: Proc. ISBI. pp. 1119–1122 (2008)
117. Mahapatra, D., Sun, Y.: Using saliency features for graphcut segmentation of perfusion kidney images. In: In 13th International Conference on Biomedical Engineering (2008)

118. Mahapatra, D., Sun, Y.: Joint registration and segmentation of dynamic cardiac perfusion images using mrfs. In: Proc. MICCAI. pp. 493–501 (2010)
119. Mahapatra, D., Sun, Y.: An mrf framework for joint registration and segmentation of natural and perfusion images. In: Proc. IEEE ICIP. pp. 1709–1712 (2010)
120. Mahapatra, D., Sun, Y.: Retrieval of perfusion images using cosegmentation and shape context information. In: Proc. APSIPA Annual Summit and Conference (ASC) (2010)
121. Mahapatra, D., Sun, Y.: Rigid registration of renal perfusion images using a neurobiology based visual saliency model. EURASIP Journal on Image and Video Processing. pp. 1–16 (2010)
122. Mahapatra, D., Sun, Y.: A saliency based mrf method for the joint registration and segmentation of dynamic renal mr images. In: Proc. ICDIP (2010)
123. Mahapatra, D., Sun, Y.: Mrf based intensity invariant elastic registration of cardiac perfusion images using saliency information. IEEE Trans. Biomed. Engg. **58**(4), 991–1000 (2011)
124. Mahapatra, D., Sun, Y.: Orientation histograms as shape priors for left ventricle segmentation using graph cuts. In: In Proc: MICCAI. pp. 420–427 (2011)
125. Mahapatra, D., Sun, Y.: Integrating segmentation information for improved mrf-based elastic image registration. IEEE Trans. Imag. Proc. **21**(1), 170–183 (2012)
126. Mahapatra, D., Tielbeek, J., Buhmann, J., Vos, F.: A supervised learning based approach to detect crohn’s disease in abdominal mr volumes. In: Proc. MICCAI workshop Computational and Clinical Applications in Abdominal Imaging(MICCAI-ABD). pp. 97–106 (2012)
127. Mahapatra, D., Tielbeek, J., Vos, F., , J.B.: Crohn’s disease tissue segmentation from abdominal mri using semantic information and graph cuts. In: Proc. IEEE ISBI. pp. 358–361 (2013)
128. Mahapatra, D., Tielbeek, J., Vos, F., Buhmann, J.: Localizing and segmenting crohn’s disease affected regions in abdominal mri using novel context features. In: Proc. SPIE Medical Imaging (2013)
129. Mahapatra, D., Tielbeek, J., Vos, F., Buhmann, J.: Weakly supervised semantic segmentation of crohn’s disease tissues from abdominal mri. In: Proc. IEEE ISBI. pp. 832–835 (2013)
130. Mahapatra, D., Vos, F., Buhmann, J.: Crohn’s disease segmentation from mri using learned image priors. In: In Proc. IEEE ISBI. pp. 625–628 (2015)
131. Mahapatra, D., Vos, F., Buhmann, J.: Active learning based segmentation of crohns disease from abdominal mri. Computer Methods and Programs in Biomedicine **128**(1), 75–85 (2016)
132. Mahapatra, D., Winkler, S., Yen, S.: Motion saliency outweighs other low-level features while watching videos. In: SPIE HVEI. pp. 1–10 (2008)
133. Mahapatra, D.: Registration and segmentation methodology for perfusion mr images: Application to cardiac and renal images. - pp. - (2011)
134. Mahapatra, D.: Registration and segmentation methodology for perfusion mr images: Application to cardiac and renal images. - pp. - (2011)
135. Mahapatra, D., Poellinger, A., Shao, L., Reyes, M.: Interpretability-driven sample selection using self supervised learning for disease classification and segmentation. IEEE TMI pp. 1–15 (2021)
136. Min, S., Yao, H., Xie, H., Wang, C., Zha, Z.J., Zhang, Y.: Domain-aware visual bias eliminating for generalized zero-shot learning. In: The IEEE Conference on Computer Vision and Pattern Recognition (CVPR). pp. 12664–12673 (June 2020)
137. Mnih, A., Kavukcuoglu, K.: Learning word embeddings efficiently with noise-contrastive estimation. In: In Proc. NeurIPS. p. 2265–2273 (2013)



138. Nair, V., Hinton, G.E.: Rectified linear units improve restricted boltzmann machines. In: In Proc. ICML. pp. 807–814 (2010)
139. Nyul, L., Udupa, J., Zhang, X.: New variants of a method of mri scale standardization. *IEEE Trans. Medical Imaging* **19**(2), 143–150 (2000)
140. van den Oord, A., Li, Y., Vinyals, O.: Representation learning with contrastive predictive coding. In: arXiv:1807.03748 (2018)
141. Pandey, A., Paliwal, B., Dhall, A., Subramanian, R., Mahapatra, D.: This explains that: Congruent image–report generation for explainable medical image analysis with cyclic generative adversarial networks. In: In MICCAI-iMIMIC 2021. pp. 1–11 (2021)
142. Roy, P., Chakravorty, R., Sedai, S., Mahapatra, D., Garnavi, R.: Automatic eye type detection in retinal fundus image using fusion of transfer learning and anatomical features. In: In Proc. DICTA. pp. 1–7 (2016)
143. Roy, P., Tennakoon, R., Cao, K., Sedai, S., Mahapatra, D., Maetschke, S., Garnavi, R.: A novel hybrid approach for severity assessment of diabetic retinopathy in colour fundus images,. In: In Proc. IEEE ISBI. pp. 1078–1082 (2017)
144. Roy, P., Mahapatra, D., Garnavi, R., Tennakoon, R.: System and method to teach and evaluate image grading performance using prior learned expert knowledge base. In: US Patent App. 10,984,674 (2021)
145. Rusu, M., Shao, W., Kunder, C.A., Wang, J.B., Soerensen, S.J.C., et al.: Registration of pre-surgical mri and histopathology images from radical prostatectomy via rapsodi. *Medical Physics* **47**(9), 4177–4188 (2020)
146. Saini, M., Guthier, B., Kuang, H., Mahapatra, D., Saddik, A.: szoom: A framework for automatic zoom into high resolution surveillance videos. In: arXiv preprint arXiv:1909.10164 (2019)
147. Schüffler, P., Mahapatra, D., Tielbeek, J., Vos, F., Makanyanga, J., Pends, D., Nio, C., Stoker, J., Taylor, S., Buhmann, J.: A model development pipeline for crohns disease severity assessment from magnetic resonance images. In: In Proc: MICCAI-ABD (2013)
148. Schüffler, P., Mahapatra, D., Tielbeek, J., Vos, F., Makanyanga, J., Pends, D., Nio, C., Stoker, J., Taylor, S., Buhmann, J.: Semi automatic crohns disease severity assessment on mr imaging. In: In Proc: MICCAI-ABD (2014)
149. Schuffler, P.J., Mahapatra, D., Vos, F., Buhmann, J.: Computer aided crohn’s disease severity assessment in mri. In: VIGOR++ Workshop 2014-Showcase of Research Outcomes and Future Outlook. pp. – (2014)
150. Sedai, S., Mahapatra, D., Antony, B., Garnavi, R.: Joint segmentation and uncertainty visualization of retinal layers in optical coherence tomography images using bayesian deep learning. In: In Proc. MICCAI-OMIA. pp. 219–227 (2018)
151. Sedai, S., Mahapatra, D., Ge, Z., Chakravorty, R., Garnavi, R.: Deep multiscale convolutional feature learning for weakly supervised localization of chest pathologies in x-ray images. In: In Proc. MICCAI-MLMI. pp. 267–275 (2018)
152. Sedai, S., Mahapatra, D., Hewavitharanage, S., Maetschke, S., Garnavi, R.: Semi-supervised segmentation of optic cup in retinal fundus images using variational autoencoder,. In: In Proc. MICCAI. pp. 75–82 (2017)
153. Sedai, S., Roy, P., Mahapatra, D., Garnavi, R.: Segmentation of optic disc and optic cup in retinal fundus images using shape regression. In: In Proc. EMBC. pp. 3260–3264 (2016)
154. Sedai, S., Roy, P., Mahapatra, D., Garnavi, R.: Segmentation of optic disc and optic cup in retinal images using coupled shape regression. In: In Proc. MICCAI-OMIA. pp. 1–8 (2016)

155. Srivastava, S., Yaqub, M., Nandakumar, K., Ge, Z., Mahapatra, D.: Continual domain incremental learning for chest x-ray classification in low-resource clinical settings. In: In MICCAI-FAIR 2021. pp. 1–11 (2021)
156. Tennakoon, R., Mahapatra, D., Roy, P., Sedai, S., Garnavi, R.: Image quality classification for dr screening using convolutional neural networks. In: In Proc. MICCAI-OMIA. pp. 113–120 (2016)
157. Tong, J., Mahapatra, D., Bonnington, P., Drummond, T., Ge, Z.: Registration of histopathology images using self supervised fine grained feature maps. In: In Proc. MICCAI-DART Workshop. pp. 41–51 (2020)
158. Verma, R., Kumar, N., Patil, A., et. al.: Monusac2020: A multi-organ nuclei segmentation and classification challenge. IEEE TMI pp. 1–14 (2021)
159. Vos, F.M., Tielbeek, J., Naziroglu, R., Li, Z., Schüffler, P., Mahapatra, D., Wiebel, A., Lavini, C., Buhmann, J., Hege, H., Stoker, J., van Vliet, L.: Computational modeling for assessment of IBD: to be or not to be? In: Proc. IEEE EMBC. pp. 3974–3977 (2012)
160. Wu, J., Zhang, T., Zha, Z.J., Luo, J., Zhang, Y., Wu, F.: Self-supervised domain-aware generative network for generalized zero-shot learning. In: The IEEE Conference on Computer Vision and Pattern Recognition (CVPR). pp. 12767–12776 (June 2020)
161. Xian, Y., Lorenz, T., Schiele, B., Akata, Z.: Feature generating networks for zero-shot learning. In: In Proc. IEEE CVPR. pp. 5542–5551 (2018)
162. Xing, Y., Ge, Z., Zeng, R., Mahapatra, D., Seah, J., Law, M., Drummond, T.: Adversarial pulmonary pathology translation for pairwise chest x-ray data augmentation. In: In Proc. MICCAI. pp. 757–765 (2019)
163. Zhu, J.Y., Park, T., Isola, P., Efros, A.A.: Unpaired image-to-image translation using cycle-consistent adversarial networks. In: arXiv preprint arXiv:1703.10593 (2017)
164. Zilly, J., Buhmann, J., Mahapatra, D.: Boosting convolutional filters with entropy sampling for optic cup and disc image segmentation from fundus images. In: In Proc. MLMI. pp. 136–143 (2015)
165. Zilly, J., Buhmann, J., Mahapatra, D.: Glaucoma detection using entropy sampling and ensemble learning for automatic optic cup and disc segmentation. In Press Computerized Medical Imaging and Graphics **55**(1), 28–41 (2017)